

# Subsurface characterization of high dielectric nanostructures in low dielectric polymer matrix using Electric Force Microscopy and Scanning Electron Microscopy

Minhua Zhao<sup>1</sup>, Bin Ming<sup>2</sup>, Andras E. Vladar<sup>2</sup>, Paul Stutzman<sup>1</sup>, Guodong Chen<sup>1</sup>, Xiaohong Gu<sup>1</sup>, Cheol Park<sup>3</sup>, Y.C. Jean<sup>4</sup>, and Tinh Nguyen<sup>1</sup>

<sup>1,2</sup>National Institute of Standards and Technology, Gaithersburg, MD 20899, <sup>1</sup>Materials and Construction Research Division, <sup>2</sup>Precision Engineering Division, <sup>3</sup>National Institute of Aerospace, Hampton, <sup>4</sup>Department of Chemistry, University of Missouri, Kansas City

## ABSTRACT

Scanning Probe Microscopy (SPM) and Scanning Electron Microscopy (SEM) are two powerful techniques for surface characterization of nanostructures. With the development of nanotechnology, there is a growing need to nondestructively characterize nanostructures at the *subsurface* of materials, such as dispersion of carbon nanotubes (CNTs) in polymer composites, which is beyond the capabilities of conventional SPM and SEM techniques. Here we report subsurface characterization of CNTs in polyimide composites using Electric Force Microscopy (EFM), a special type of SPM based on long-range electrostatic interactions; and Poly-Transparent SEM (PT-SEM) based on the charge contrast at the interface of CNTs and polymers. The effectiveness of these techniques is demonstrated by subsurface imaging of polyimide nanocomposites containing different concentrations of CNTs using EFM technique alone and combined EFM and PT-SEM techniques at the same location of the sample. Key experimental parameters are studied and a new contrast mechanism for EFM and SEM subsurface imaging of CNTs in polymer matrix is proposed. Furthermore, these techniques can be universally applied to characterize high dielectric nanostructures in low dielectric matrices, with a broad range of applications in nanotechnology.

**Keywords:** electric force microscopy, scanning electron microscopy, nanocomposites, subsurface, carbon nanotube.

## 1 INTRODUCTION

Scanning Probe Microscopy (SPM) and Scanning Electron Microscopy (SEM) are two complementary techniques for high resolution surface characterization. SPM is a branch of microscopy that forms images of surfaces using a physical probe that scans the specimen. An image of the surface is obtained by mechanically moving the probe in a raster scan of the specimen, line by line, and recording the probe-surface interaction as a function of position. The main advantage of a SPM is that samples can be observed in air or liquid environments without the need for partial vacuum. In comparison, SEM is a type of electron microscopy that images the sample surface by scanning it with a high-energy beam of electrons in a raster

scan pattern. The main advantages of SEM over SPM include: (i) much faster scan speed and much larger scan area; (ii) compositional information through x-ray energy-dispersive spectroscopy. With the advent of nanotechnology, there is also a growing need for high resolution subsurface, e.g., understanding the dispersion of carbon nanotubes (CNTs) in a polymer matrix is critical for improving the performance of nanocomposites. While conventional SPM and SEM are mainly used for surface characterization, two specific techniques named Electric Force Microscopy (EFM) [1] and Poly-Transparent SEM (PT-SEM) [2], are promising for high resolution subsurface characterization. EFM is a special type of SPM technique based on long-range electrostatic interactions between a probe and a sample for the characterization of local electronic and/or dielectric properties of insulating, conducting and semi-conducting materials. For instance, EFM was used for subsurface imaging of CNTs dispersed in polymer composites [3]. PT-SEM was also applied to provide a quantitative assessment of CNT dispersion in a polymer matrix through the use of an electric field or charge contrast [2]. In this study, subsurface imaging of polyimide nano-composites containing different concentrations of CNTs is conducted using EFM alone and combined EFM and PT-SEM techniques at the same location in the sample. Key experimental parameters are studied and a new contrast mechanism for subsurface imaging of CNTs in polymer matrix is proposed.

## 2 EXPERIMENTS\*

Single wall carbon nanotube (SWCNT)-polyimide nanocomposite films were prepared by in-situ polymerization as described previously [4]. The purified laser ablated (LA) and high-pressure carbon monoxide decomposition (HIPCO) SWCNTs were purchased from Rice University and Carbon Nanotechnologies, Inc., respectively. The polymer matrix was a transparent polyimide (CP2). As-received anhydrous dimethyl formamide (DMF, Fisher Scientific) was used as a solvent. A series of SWCNT-polyimide nanocomposite films with SWCNT concentrations at mass fractions of (0, 0.05, 0.2, 0.5, 2 and 10) % were prepared as follows. The SWCNT-poly(amic acid) solution was cast onto a glass plate, dried in a dry air-flowing chamber and peeled from the glass

substrate. Subsequently, the dried tack-free film was thermally imidized in a nitrogen-circulating oven to obtain a solvent-free SWCNT-polyimide film having a thickness between 25  $\mu\text{m}$  and 65  $\mu\text{m}$ . The smoother interface side (glass-film interface) was used for EFM and SEM imaging.

Figure 1 is a schematic of the EFM setup for subsurface imaging of nanofillers in polymer films based on two-pass scanning techniques. During the first pass, the topographic image was acquired in normal tapping mode using a Veeco Dimension 3100 Atomic Force Microscopy (AFM) equipped with Nanoscope IV controller. The second pass raised the conductive AFM probe above the sample to a fixed distance and re-scanned the surface with a bias voltage applied between the probe and AFM stage, following the previous-recorded topography to maintain a constant tip-sample separation. The amplitude and phase of the probe during the second pass were recorded as EFM signals. The bias voltage applied to the AFM probes ranged from -12 V to +12 V and the lift height was kept at 20 nm. The EFM imaging was carried out using the NIST-patented (US 6.490.913 B1) environmental chamber that was custom-designed and fabricated for the Dimension 3100 AFM.

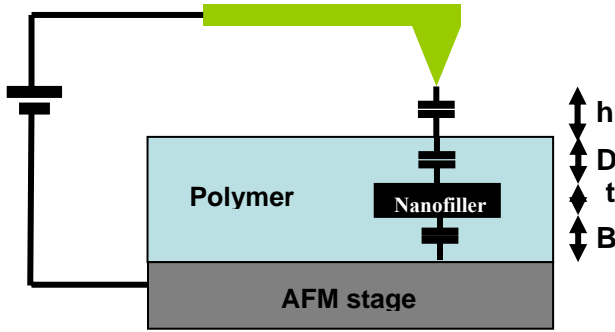


Figure 1: Schematic of EFM setup for subsurface characterization of nanofillers in a free-standing polymer composite film.

The capacitive electrostatic force between the probe and sample is given by Equation (1).

$$F = \frac{1}{2} \frac{dC}{d\lambda} V_{tip}^2 \quad (1)$$

where  $F$  is the electrostatic force,  $C$  is the capacitance between the tip and sample,  $\lambda$  is the tip-sample distance, and  $V_{tip}$  is the bias voltage on the tip. The change in phase shift,  $\Delta\Phi$ , of the vibrating AFM probe defined by Equation (2) is recorded pixel by pixel to form an EFM image during the second pass under the approximation of a harmonic oscillator [5, 6] using a conventional capacitive coupling model:

$$\Delta\Phi = \Phi - \Phi_0 \approx \tan(\Phi - \Phi_0) \approx \frac{Q}{k} F' = \frac{Q}{2k} (C_1''(z) - C_2''(z)) V_{tip}^2 \quad (2)$$

where  $\Phi$  is the phase shift when the probe is over the nanofiller (Figure 1),  $\Phi_0$  is the phase shift when the probe is over the unfilled film,  $Q$  is the quality factor of the AFM

probe, and  $k$  is the spring constant of the AFM probe. Assuming a plane-capacitor model [5], Equation (3) describes the second derivative of the tip-nanofiller capacitance,  $C_2''(z)$ , and Equation (4) describes the second derivative of the tip-polymer film capacitance,  $C_1''(z)$ ,

$$C_2''(z) = 8\pi\epsilon_0 \left[ \ln\left(\frac{1+\cos\theta}{1-\cos\theta}\right) \right]^{-2} \frac{1}{\{h+(D+B)/\epsilon_{film} + t/\epsilon_{filler}\}^3} \quad (3)$$

$$C_1''(z) = 8\pi\epsilon_0 \left[ \ln\left(\frac{1+\cos\theta}{1-\cos\theta}\right) \right]^{-2} \frac{1}{\{h+(D+B+t)/\epsilon_{film}\}^3} \quad (4)$$

where  $\epsilon_0$  is the permittivity constant,  $\theta$  is the AFM tip cone half angle,  $h$  is the distance between tip apex and top surface of the film,  $D$  is the depth of the nanofiller located from the film top surface,  $z$  ( $=h+D$ ) is the tip-nanofiller distance,  $B$  is the distance of the nanofiller to the bottom of the film,  $t$  is the thickness of the nanofiller,  $\epsilon_{filler}$  is the permittivity of the filler, and  $\epsilon_{film}$  is the permittivity of the unfilled polymer matrix. According to the Equations 2, 3 and 4 based on the capacitive coupling model, EFM phase contrast of nanofillers can only be revealed when the dielectric constant of the nanofillers is sufficiently different from that of the polymer matrix. However, we will demonstrate later that capacitive coupling model is not adequate to describe the EFM contrast mechanism of nanofillers embedded in polymer matrix.

The same location in the region characterized by EFM was also studied using a FEI Helios NanoLab 600 Dual-Beam system. In this experiment, the beam accelerating voltage was varied between 1 kV, 2 kV, 4 kV, 6 kV, 8 kV and 15 kV, while the beam current was maintained at 43 pA, with the sample at 4.3 mm working distance. Collected SEM images had a horizontal width of 1024 pixels and a height of 768 pixels. A beam dwell time of 40  $\mu\text{s}$  was used for each image pixel. These parameters were used throughout the study to obtain image-to-image consistency.

### 3 RESULTS AND DISCUSSIONS

#### 3.1 EFM for subsurface characterization

Figure 2 shows subsurface EFM images of SWCNT-polyimide nanocomposite films with different SWCNT loadings. The left, middle and right columns of Figure 2 are height, AFM phase and EFM phase images, respectively. Neither the height nor the conventional AFM phase images show the dispersion of SWCNTs in the film. However, as the SWCNT loadings are increased from 0.05 % to 10 % in the film, more curved line features with dark phase contrast are revealed in the EFM images. Moreover, the control sample CNT-free polyimide film does not have any line features with negative contrast (not shown). Because the dielectric constant of SWCNTs is much higher than that of the polyimide ( $\cong 4$ ), it is reasonable to obtain negative EFM contrast when SWCNTs are dispersed in the polyimide matrix [3].

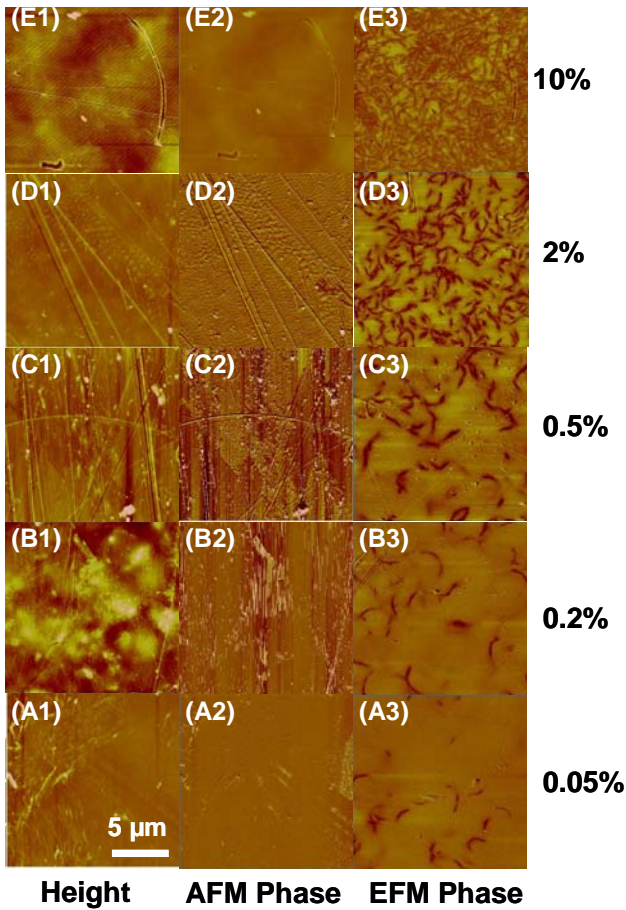


Figure 2: EFM subsurface imaging of SWCNT (HIPCO) - polyimide composites with SWCNT mass fraction of (A) 0.05 %, (B) 0.2 %, (C) 0.5 %, (D) 2 % and (E) 10 %. Left column: Height, scale 50 nm. Middle column: AFM phase, scale 40°. Right column: EFM phase, scale 40°.

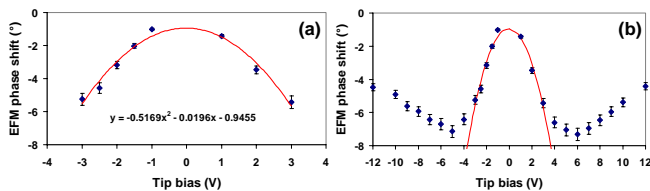


Figure 3: Effect of the bias voltage on the EFM phase signal. (a) Relationship of EFM phase signal to the bias voltage in the range of -3 V to +3V. The line is a theoretical fitting by parabolic law. (b) Relationship of EFM phase signal to the bias voltage in the range of -12 V to +12 V. The line is the same parabolic fitting in (a). Uncertainty bars represent one standard deviation.

A key parameter for EFM subsurface imaging is the applied voltage between the probe and sample. The characteristic parabolic shape of phase shift vs. tip bias is observed at low bias range (Figure 3a), which conforms to the conventional model of capacitive coupling between the

probe and sample as defined by Equation (2). However, at a higher bias, the voltage dependence of EFM phase shift is no longer parabolic as shown in Figure 3b. More interestingly, the EFM phase shift is even reduced with the increase of bias voltage beyond a certain threshold, which is dependent on the sample and lift height. These experimental findings cannot be explained by the conventional capacitive coupling defined by Equation (2). Hence, a new mechanism to explain the voltage dependence of EFM phase contrast is required. Since most of the previous EFM work dealt with conductive samples, there is little understanding of EFM contrast mechanisms between high dielectric constant nanostructures (e.g., CNTs) and a low dielectric constant matrix (e.g., polymer film). When a biased tip is placed very close to a low dielectric film, charge injection into the film is possible [7]. The effect of charge injection on the EFM signal [8, 9] can be accounted for using Equations (5) & (6),

$$F_{\text{Electrostatic}} = F_{\text{Capacitive}} + F_{\text{Coulombic}} = \frac{V^2}{2} \frac{\partial C}{\partial z} - \frac{Q_s C V}{4\pi\epsilon_0 z^2} - \frac{Q_s^2}{4\pi\epsilon_0 z^2} \quad (5)$$

$$\Delta\phi \propto \frac{\partial F}{\partial z} = \frac{V^2}{2} \frac{\partial^2 C}{\partial z^2} + \frac{Q_s V}{2\pi\epsilon_0 z^2} \left[ \frac{C}{z} - \frac{1}{2} \frac{\partial C}{\partial z} \right] + \frac{Q_s^2}{2\pi\epsilon_0 z^3} \quad (6)$$

where  $V$  is the bias voltage,  $C$  is the capacitance between the tip and sample,  $z$  is the tip-sample distance,  $Q_s$  is charge injected into the sample and  $\epsilon_0$  is the permittivity constant. Electrostatic interactions between the probe and sample are comprised of capacitive and coulombic coupling. The first term in Equation (5) accounts for capacitive coupling, while the others are related to coulombic coupling. If the injected charge  $Q_s$  and/or tip-sample capacitance  $C$  is voltage dependent [10, 11], the relationship between EFM phase shift  $\Delta\Phi$  and tip bias  $V$  will no longer be parabolic according to Equation (6), which can explain why the EFM contrast could even be reduced at large tip bias as shown in Figure 3b. Furthermore, the EFM contrast (top row) of CNTs in polymer composites changed from dark to bright with an increase of the tip bias voltage as shown in Figure 4. Interestingly, similar inversion of SEM contrast was observed on CNTs when the SEM acceleration voltage was increased, which will be shown later.

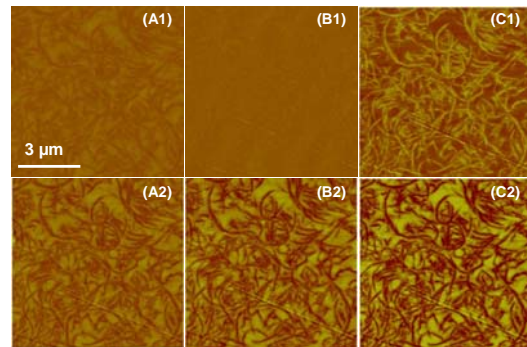


Figure 4: Inversion of EFM contrast of CNTs in 10 % SWCNT (HIPCO)-polyimide composite film by bias

voltage at lift height of 20 nm. Top row: EFM amplitude signal with 100 mV scale. Bottom row: EFM phase signal with 20° scale. (A1)&(A2): -3 V bias; (B1)&(B2): -4 V bias; (C1)&(C2): -5 V bias.

### 3.2 Combined EFM and PT-SEM

Figure 5 shows the combined EFM and PT-SEM subsurface imaging of CNT-polyimide composites at the same location. While conventional SPM height image (Fig.5a) could not detect the subsurface CNTs, both EFM (Fig.5b) and PT-SEM (Figs.5c-5d) can reveal the CNTs embedded below the surface. Furthermore, the PT-SEM contrast of CNTs was reversed from dark to bright with the increase of acceleration voltage, similar to what was observed in EFM imaging (Fig. 4). It is hypothesized that the contrast mechanism of subsurface imaging of CNTs by PT-SEM is related to the charge accumulated or dissipated at the interface between the CNTs and polymer matrix. The similarity of PT-SEM and EFM contrast reverse implies that there is a common mechanism for both techniques, in which the interface of CNT/polymer may play an important role in charge accumulation and dissipation during subsurface imaging. It is worth mentioning that PT-SEM only works when the conductivity of the sample is within a certain range ( $\sim 10^{-7}$ - $10^{-1}$  S/m) and no conductive coating is applied at the surface. Furthermore, more subsurface CNTs are revealed at higher SEM acceleration voltage (Figs.5c & d), which is due to deeper electron-sample interaction region at higher acceleration voltage. More research is going on to verify this mechanism postulation.

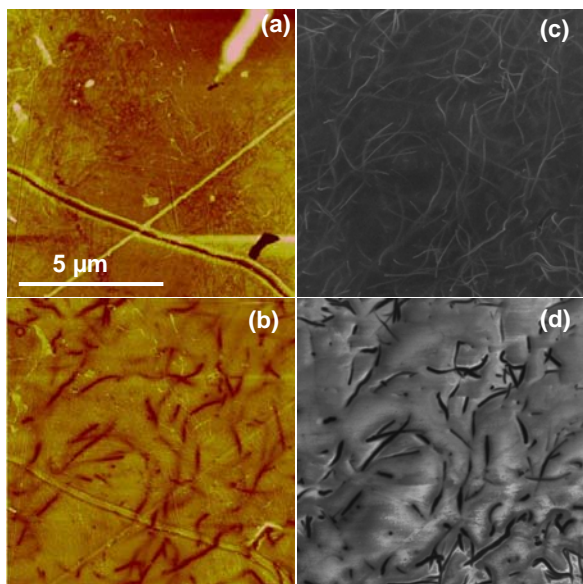


Figure 5: Combined EFM and PT-SEM subsurface imaging at the same location of SWCNT(LA)-polyimide composite film. (a) AFM height scale 50 nm, (b) EFM phase scale 20°, (c) SEM image at acceleration voltage of 8 kV, (d) SEM image at acceleration voltage of 1 kV.

## 4 CONCLUSIONS

Both EFM and PT-SEM have been successfully applied to characterize the CNTs dispersed in the subsurface regions of a nanocomposite. A new contrast mechanism based on interface charge accumulation and dissipation has been proposed to account for the experimental findings. These techniques can be universally applied to characterize high dielectric nanostructures embedded in low dielectric matrix, with a broad range of applications in nanotechnology. Further optimization of these techniques is ongoing.

## REFERENCES

1. Zhao, M.H., et al., *Nanotechnology*. **19**, 235704, 2008.
2. Lillehei, P.T., et al., *Nanotechnology*. **20**, 325708, 2009.
3. Zhao, M.H., et al., *Nanotechnology*. **submitted**, 2010.
4. Park, C., et al., *Chemical Physics Letters*. **364**, 303, 2002.
5. Bockrath, M., et al., *Nano Letters*. **2**, 187, 2002.
6. Staii, C., A.T. Johnson, and N.J. Pinto, *Nano Letters*. **4**, 859, 2004.
7. Terris, B.D., et al., *Journal of Vacuum Science & Technology a-Vacuum Surfaces and Films*. **8**, 374, 1990.
8. Baird, P.J.S., J.R. Bowler, and G.C. Stevens. *Quantitative methods for non-contact electrostatic force microscopy*. **163**, 381, 1999.
9. Jespersen, T.S. and J. Nygard, *Nano Letters*. **5**, 1838, 2005.
10. Dragoman, D. and M. Dragoman, *Journal of Applied Physics*. **101**, 3, 2007.
11. Heo, J.S. and M. Bockrath, *Nano Letters*. **5**, 853, 2005.

---

\* Certain commercial equipment, instruments, or materials are identified in this paper to foster understanding. Such identification does not imply recommendation or endorsement by the National Institute of Standards and Technology, nor does it imply that the materials or equipment identified are necessarily the best available for the purpose.